

Graph Similarity Description: How Are These Graphs Similar?

Corinna Coupette

Max Planck Institute for Informatics
Saarbrücken, Germany
coupette@mpi-inf.mpg.de

Jilles Vreeken

CISPA Helmholtz Center for Information Security
Saarbrücken, Germany
jv@cispa.de

ABSTRACT

How do social networks differ across platforms? How do information networks change over time? Answering questions like these requires us to compare two or more graphs. This task is commonly treated as a *measurement* problem, but numerical answers give limited insight. Here, we argue that if the goal is to gain understanding, we should treat graph similarity assessment as a *description* problem instead. We formalize this problem as a model selection task using the Minimum Description Length principle, capturing the similarity of the input graphs in a *common model* and the differences between them in *transformations* to *individual models*. To discover good models, we propose MOMO, which breaks the problem into two parts and introduces efficient algorithms for each. Through an extensive set of experiments on a wide range of synthetic and real-world graphs, we confirm that MOMO works well in practice.

CCS CONCEPTS

• **Information systems** → **Data mining**; • **Mathematics of computing** → **Exploratory data analysis**; **Graph algorithms**.

KEYWORDS

Graph Similarity; Graph Summarization; Information Theory

ACM Reference Format:

Corinna Coupette and Jilles Vreeken. 2021. Graph Similarity Description: How Are These Graphs Similar?. In *Proceedings of the 27th ACM SIGKDD Conference on Knowledge Discovery and Data Mining (KDD '21), August 14–18, 2021, Virtual Event, Singapore*. ACM, New York, NY, USA, 11 pages. <https://doi.org/10.1145/3447548.3467257>

1 INTRODUCTION

Comparing two or more graphs is important in many applications. In biology, we might, for example, want to compare the protein interaction networks of different human tissues so as to discover common and specialized mechanisms, while in the social sciences, comparing collaboration networks over time or across fields could reveal knowledge dynamics. The task of comparing graphs is called *graph similarity assessment*. It is commonly treated as a *measurement* problem, i.e., a question to which a numerical answer suffices (e.g., 0.42). While such an answer may be useful in certain downstream tasks like classification or clustering, it provides limited insight and is thus generally dissatisfying to a domain expert.



This work is licensed under a Creative Commons Attribution International 4.0 License.

KDD '21, August 14–18, 2021, Virtual Event, Singapore.

© 2021 Copyright held by the owner/author(s).

ACM ISBN 978-1-4503-8332-5/21/08.

<https://doi.org/10.1145/3447548.3467257>

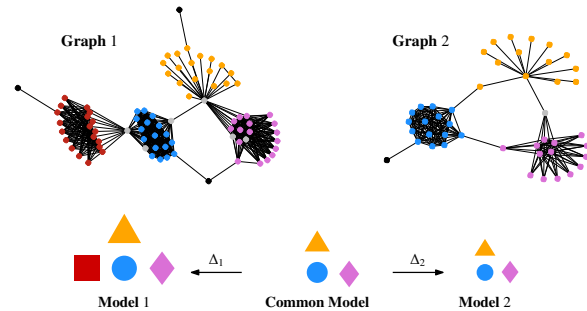


Figure 1: A common model captures the structure shared between the individual models of the input graphs.

In this paper, we argue that if the goal is to gain understanding, we should not ask “how *similar* are these graphs?” but rather “how are these graphs similar?”. That is, we propose to treat graph similarity assessment as a *description* problem, demanding an answer that, in easily understandable terms, characterizes what is similar and what is different between the input graphs at hand. We formalize the problem in information-theoretic terms using the Minimum Description Length (MDL) principle, by which we are after the shortest lossless description of the input graphs using common and specific structures (e.g., stars, cliques, bicliques, and starcliques) as well as shared nodes and edges between these structures. Since we can measure how many bits we gain by compressing the graphs jointly, rather than individually, our formalization also allows for an easily interpretable quantification of differences.

As an example of graph similarity description, consider Figure 1, which depicts two toy graphs and the result returned by our method. Even though the graphs are of different sizes, and no node alignment is given, our method discovers that both graphs contain a star (orange triangle) that is connected to a clique (blue circle) and a starclique (pink diamond). We further see that the left graph is different in that it additionally contains a biclique (red square), and that the structures in the left graph all contain more nodes than their counterparts in the right graph (larger shapes).

When assessing the similarity between graphs in practice, we face a very large search space: There exist exponentially many sets of nodes, i.e., potential structures, exponentially many *sets* of structures, and—unless a full node alignment is given—also exponentially many alignments between the graphs. As our score exhibits no structure that we could exploit to efficiently discover the optimal solution, we propose a framework, called MOMO (*Model of models*), that breaks the problem into two parts and introduces efficient algorithms for each: BEPPO discovers interpretable summaries for the individual input graphs, and GIGI uses them to unveil their shared and specific structures, from which we can also compute an informative similarity score. Through an extensive set of experiments on

a wide range of synthetic and real-world graphs, we confirm that our algorithms perform well in practice: We discover summaries that are useful for domain experts, identify meaningful similarities between the protein interaction networks of different human tissues, and reveal distinct temporal dynamics in the collaboration networks of different scientific communities. Not unimportantly, in practice, our methods scale near-linearly in the number of edges.

The remainder of the paper is structured as follows. Section 2 introduces our notation and gives a primer on MDL, and Sections 3, 4, and 6 present our main contributions. We cover related work in Section 5, and round up with discussion and conclusions in Section 7. All our data, code, and results are publicly available,¹ and further information for reproducibility is given in Appendix A.

2 PRELIMINARIES

We consider graphs $G_i = (V_i, E_i)$ with $n_i = |V_i|$ nodes, $m_i = |E_i|$ edges, and adjacency matrix A_i , omitting the subscripts when clear from context. An alignment \mathcal{A}_{ij} between the graphs G_i and G_j , denoted $G_i \parallel_{\mathcal{A}} G_j$, is a bijection from V_i to V_j . To allow comparisons between graphs of different sizes or graphs for which no node alignment is known, we allow this bijection to be *partial* or *empty*, i.e., there can be nodes in V_i (V_j) that have no image (preimage) in V_j (V_i) under \mathcal{A}_{ij} . We assume that our input graphs are *simple*, i.e., undirected, unweighted, without loops or parallel edges, and that only *two* input graphs are given, but our framework generalizes to comparisons between *more than two general* graphs.

We build on the notion of *Kolmogorov complexity*. The Kolmogorov complexity of an object x , $K(x)$, is the length in bits of the shortest program computing x on a universal Turing machine, and the *conditional* Kolmogorov complexity of x given y , $K(x | y)$, is the length of such a program with y as auxiliary input [17]. The *Information Distance* between x and y is (up to an additive logarithmic term) the length of the shortest program transforming x into y and y into x , i.e., $ID(x, y) = \max\{K(x | y), K(y | x)\}$ [16]. Dividing by $\max\{K(x), K(y)\}$, we obtain the *Normalized Information Distance*.

The Kolmogorov complexity is not computable, and hence, neither is the Normalized Information Distance. To *describe* and *measure* the similarity between graphs in practice, we thus instantiate Kolmogorov complexity through the Minimum Description Length (MDL) principle [10]. MDL is a practical version of Kolmogorov complexity embracing the slogan *Induction by Compression*. Given a model class \mathfrak{M} for some data \mathcal{D} , the best model $M \in \mathfrak{M}$ minimizes $L(M) + L(\mathcal{D} | M)$, where $L(M)$ is the description length of M , $L(\mathcal{D} | M)$ is the description length of the data when encoded using M , and both are measured in bits under our encoding. This is called *crude* MDL, and it contrasts with *refined* MDL, which encodes the model and the data together [10]. We opt for crude MDL not only because it is computable but also because we are particularly interested in the model: the structures shared by our input graphs, and the transformations necessary to derive the individual graphs from them. Finally, we require *lossless* descriptions to ensure fair comparisons between competing models.

All logarithms are to base 2, and we define $\log 0 = 0$. We use $\lfloor \cdot \rfloor$ for rounding to the closest integer, and summarize our notation in Table 2 in the Appendix.

¹<http://eda.mmci.uni-saarland.de/prj/momo>; <https://doi.org/10.5281/zenodo.4780912>

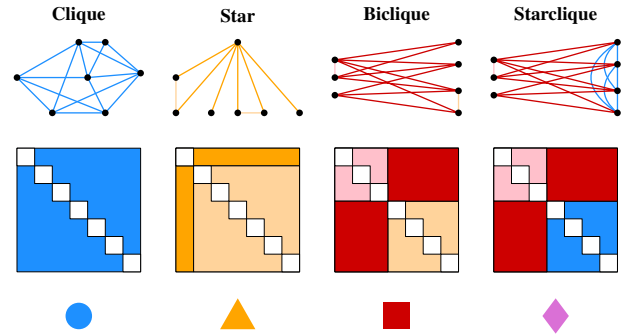


Figure 2: Graph structures are constraints over sets of (non-) edges. They can be visualized as induced subgraphs (top), adjacency submatrices (middle), or shapes (bottom). Each color in the adjacency submatrix is associated with a different constraint, where the white constraint enforces loop-freeness.

3 THEORY

We now describe our first contribution, the MDL formulation of graph similarity assessment. Our data is $\mathcal{D} = (G_1, G_2, \mathcal{A})$, where G_1 and G_2 are our input graphs, and \mathcal{A} is a (potentially partial or empty) node alignment between G_1 and G_2 .

3.1 Similarity Description, Informally

Our primary goal is to *describe* the similarity of our input graphs. That is, we aim to find the key structures that are shared between these graphs and contrast them with the structures that are specific to the individual graphs. By *structures*, we mean subgraphs whose connectivity follows distinct, interpretable patterns. Our *structure vocabulary* Ω comprises four structure types: (approximate) *cliques*, *stars*, *bicliques*, and *starcliques*. We choose these structure types because they are simple and widespread in real-world graphs from many different fields, but further structure types can easily be included, e.g., to tailor our method to a particular domain.

Intuitively, *cliques* are subgraphs with relatively homogeneous connectivity whose density stands out against the background distribution (e.g., echo chambers in social networks). *Stars* are subgraphs in which one node, the *hub*, is connected to all other nodes, the *spokes*, and the spokes are hardly connected among themselves (e.g., influencers and their followers). *Bicliques* are subgraphs whose nodes can be partitioned into two sets, *left* (L) and *right* (R), such that L and R are densely connected, the nodes in L are sparsely interconnected, and the nodes in R are sparsely interconnected (e.g., predators and prey in food webs). *Starcliques* are bicliques whose left nodes are densely, rather than sparsely, interconnected—i.e., stars whose hub is a clique (e.g., core and periphery in infrastructure networks). To describe real-world graphs accurately, we allow structures to overlap on nodes *and* on edges.

As depicted in Figure 2, each structure imposes a set of constraints on the connectivity in the adjacency submatrix it identifies. We think of the node set sizes of a structure as *node fractions* (relative to a reference n) and of its connectivity constraints as *edge densities* (relative to the maximum possible number of edges).

We represent the structures we find in G_1 and G_2 individually as lists S_1 and S_2 in their *individual models* M_1 and M_2 , and the structures that are shared between G_1 and G_2 as a list S_{12} in their

common model M_{12} . To decide which structures to include in S_{12} , we construct a matching $\mathcal{M} \subseteq S_1 \times S_2$, requiring that matched structures have the same type. For each $(s_1, s_2) \in \mathcal{M}$, we include one structure s of its type in S_{12} , writing $\varphi_1(s) = s_1$ and $\varphi_2(s) = s_2$ for the mappings from the shared structures to their counterparts. The node fractions (edge densities) of s are the averages of the node fractions (edge densities) in s_1 and s_2 . For example, if $s_1 \in S_1$ is a clique with node fraction 0.1 and edge density 0.9, and $s_2 \in S_2$ is a clique with node fraction 0.2 and edge density 0.7, $s \in S_{12}$ is a clique with node fraction 0.15 and edge density 0.8.

To link the common model to the individual models, we translate M_{12} into M_1 and M_2 using transformations Δ_1 and Δ_2 , i.e., $\Delta_1(M_{12}) = M_1$ and $\Delta_2(M_{12}) = M_2$. Our transformation vocabulary Σ contains edit operations to (1) add unmatched structures contained in individual models, and (2) morph structures from M_{12} into those from M_1 and M_2 , i.e., reverse the averaging we perform when specifying the shared structures. For example, if a clique $s \in S_{12}$ has node fraction 0.15 and edge density 0.8, and $\varphi_1(s) = s_1 \in S_1$ has node fraction 0.1 and edge density 0.9, we need to *shrink* the node fraction and *grow* the edge density of s to match those in s_1 .

To discover our common model M_{12} , individual models M_1 , M_2 , and transformations Δ_1 , Δ_2 , we leverage the MDL principle. We seek to optimize $L(M_{12}) + L(\Delta_1, \Delta_2) + L(G_1 \parallel_{\mathcal{A}} G_2 \mid M_{12}, \Delta_1, \Delta_2)$. For this purpose, we have to define several encodings.

3.2 Similarity Description Encodings

We need to describe how we encode (1) the graphs G_1 , G_2 under their individual models M_1 , M_2 , (2) the models M_1 , M_2 , (3) the common model M_{12} , and (4) the transformations Δ_1 , Δ_2 in bits.

Encoding a Graph Under an Individual Model. Given a model M of a graph G , rather than using an ad-hoc encoding of the graph under the model (as is common practice), we seek to encode G *optimally*, leveraging the knowledge contained in M . As depicted in Figure 2, this knowledge primarily comes as constraints on the total number of edges in the parts of the adjacency submatrix identified by the structures in M : A clique imposes one constraint, a star imposes two constraints, and a biclique or starclique imposes three constraints.

The probability distribution over the adjacency matrix \mathbf{A} of G that represents the knowledge imparted by M (which includes n , m , and loop-freeness) *without any bias* is the distribution with the largest entropy among all distributions fulfilling the constraints imposed by M . Under this *maximum entropy distribution*, $\Pr(a_{ij} \mid M) = \frac{\exp(\sum_{\lambda \in \Lambda(i,j)} \lambda)}{1 + \exp(\sum_{\lambda \in \Lambda(i,j)} \lambda)}$, where $\Lambda(i, j)$ is the set of Lagrange multipliers associated with the constraints covering $a_{ij} \in \mathbf{A}$ in the optimization problem finding the maximum entropy distribution for \mathbf{A} given M . The Shannon-optimal code based on this distribution minimizes the worst-case expected length of a message coming from the true distribution [7]. Hence, the length of G given M under an optimal encoding is

$$L(G \mid M) = \sum_{a_{ij} \in A_1} -\log \Pr(a_{ij} \mid M) + \sum_{a_{ij} \in A_0} -\log(1 - \Pr(a_{ij} \mid M)),$$

where $A_x = \{a_{ij} \in \mathbf{A} \mid (a_{ij} = x) \wedge (i < j)\}$ for $x \in \{0, 1\}$.

Encoding an Individual Model. To encode an individual model M for a graph G , we communicate n , m , and $|S|$ using $L_{\mathbb{N}}$, the universal

code for positive integers [23]. We then transmit the number of structures per type, and for each structure, in order, its type and its length. Thus, the length of an individual model M for a graph G is

$$L(M) = L_{\mathbb{N}}(n+1) + L_{\mathbb{N}}(m+1) + L_{\mathbb{N}}(|S|+1) + \log \binom{|S| + |\Omega| - 1}{|\Omega| - 1} + \sum_{s \in S} (-\log \Pr(\text{type}(s) \mid S) + L(s)).$$

Each structure is defined *abstractly* by its constraints (cf. Figure 2), and when we seek to find an MDL-optimal individual model, it is further identified by *concrete* node IDs (typeset in grey). Assuming that all structures contain a positive number of nodes, the detailed encoding of our structures is as follows.

Cliques. To communicate a clique s , we transmit its number of nodes n_s , its number of edges m_s or non-edges \bar{m}_s , and the node IDs. Therefore, with $m_s^* = n_s(n_s - 1)/2$, the length of a clique is

$$L(s) = L_{\mathbb{N}}(n_s) + 1 + \log \log \left\lceil \frac{m_s^*}{2} \right\rceil + \log(\min\{m_s, \bar{m}_s\}) + \log \binom{n}{n_s}.$$

Stars. To communicate a star s , we transmit its number of spokes $n_s - 1$, the number of edges between its spokes $x_s = m_s - n_s + 1$, the hub's ID, and the spokes' IDs. Hence, with $x_s^* = (n_s - 1)(n_s - 2)/2$, the length of a star is

$$L(s) = L_{\mathbb{N}}(n_s - 1) + \log \log x_s^* + \log x_s + \log n + \log \binom{n-1}{n_s-1}.$$

Bicliques and Starcliques. To communicate a biclique s , we transmit (1) its number of nodes n_s , (2) its number of left nodes n_L , (3) its number of edges between left nodes m_L , (4) its number of edges between right nodes m_R , (5) its number of non-edges between left nodes and right nodes $m_A^* - m_A$ (where $m_A^* := n_L n_R$), and (6) the IDs of its left nodes and its right nodes. Thus, with $m_L^* = n_L(n_L - 1)/2$ and $m_R^* = n_R(n_R - 1)/2$, the length of a biclique is

$$L(s) = L_{\mathbb{N}}(n_s) + \log n_s + \log \log m_L^* + \log m_L + \log \log m_R^* + \log m_R + \log \log m_A^* + \log(m_A^* - m_A) + \log \binom{n}{n_L} + \log \binom{n-n_L}{n_s-n_L}.$$

To transmit a starclique s , we replace m_L by $\bar{m}_L = m_L^* - m_L$.

Encoding a Common Model. When communicating M_{12} , w.l.o.g., we assume that $n_1 \geq n_2$, and we transmit the node fractions and edge densities of all shared structures with reference to n_1 . Since we explicitly want to handle unaligned graphs and graphs of different sizes, their common model does not include node IDs. To encode M_{12} , we hence use the expression for individual models, with the node ID parts omitted, and the terms for n and m replaced by

$$L_{\mathbb{N}}(n_1 + 1) + L_{\mathbb{N}}(n_1 - n_2 + 1) + L_{\mathbb{N}}(m_1 + 1) + L_{\mathbb{N}}(|m_1 - m_2| + 1) + 1.$$

Encoding Transformations. The common model M_{12} contains only structures that are shared between G_1 and G_2 , and structures may be shared without being isomorphic. Consequently, M_{12} is generally different from M_1 and M_2 , even if we define all models without node IDs. Transformations link M_{12} to M_1 and M_2 such that $\Delta_1(M_{12}) = M_1$ and $\Delta_2(M_{12}) = M_2$. That is, for $i \in \{1, 2\}$, Δ_i morphs M_{12} into M_i by *growing* or *shrinking* the node fractions and edge densities of the structures in S_{12} to match those in S_i as well as *adding* those structures from S_i that have no counterpart in S_{12} .

To derive the necessary content for the transformations, we reason as follows. The node fractions and edge densities of each structure $s \in S_{12}$ are the average of its representatives in S_1 and S_2 , $\varphi_1(s)$ and $\varphi_2(s)$. Hence, for each structure in $s \in S_{12}$, we expect a structure of the same type in S_1 and S_2 . For each node fraction x in s , we expect the size of its counterpart in $\varphi_i(s)$ to be $\lfloor x \cdot n_i \rfloor$, and for each edge density y in s , we expect the number of edges in its counterpart in $\varphi_i(s)$ to be $\lfloor y \cdot m_y^* \rfloor$, where m_y^* is the maximum number of edges in the associated area of A_i (for $i \in \{1, 2\}$).

The transformation Δ_i is the deviation of M_i from our expectation based on M_{12} , and since the node fractions and edge densities of each structure in S_{12} are the average of its representatives in S_1 and S_2 , for the shared structures, we can infer Δ_2 from Δ_1 . Hence, to communicate Δ_1 and Δ_2 , for each node fraction x (edge density y) in each structure $s \in S_{12}$, we transmit the number of nodes (edges) we need to add or subtract from $\lfloor x \cdot n_1 \rfloor$ ($\lfloor y \cdot m_y^* \rfloor$) to arrive at the size of its counterpart in $\varphi_1(s)$, along with the change direction (*grow* or *shrink*). Finally, we transmit the structures in $\bar{S}_1 := S_1 \setminus \varphi_1(S_{12})$ and the structures in $\bar{S}_2 := S_2 \setminus \varphi_2(S_{12})$.

Therefore, if $L(\delta_1 : \delta_1(s) = \varphi_1(s))$ is the description length of the transformation δ_1 morphing s into $\varphi_1(s)$, and T is the total number of change directions we need to transmit, the length of the transformations Δ_1 and Δ_2 is

$$L(\Delta_1, \Delta_2) = \sum_{s \in S_{12}} L(\delta_1 : \delta_1(s) = \varphi_1(s)) + \log T + \sum_{i \in \{1, 2\}} L_{\mathbb{N}}(|\bar{S}_i| + 1) + \sum_{i \in \{1, 2\}} \left(\log \binom{|\bar{S}_i| + |\Omega| - 1}{|\Omega| - 1} + \sum_{s \in \bar{S}_i} (-\log \Pr(\text{type}(s) \mid \bar{S}_i) + L(s)) \right).$$

Although we have defined the individual models M_1 and M_2 , the common model M_{12} , and the transformations Δ_1 and Δ_2 for similarity *description*, we can also use them for similarity *measurement*.

3.3 Similarity Measurement

For similarity measurement, our score should reflect the extent to which the structure of the input graphs can be captured by their common model. Since graphs have many permutation-invariant representations (unlike, e.g., strings), and computable instantiations of the Normalized Information Distance typically use opaque compressors, defining such a score is not straightforward. To guarantee computability and interpretability, we thus instantiate the Normalized Information Distance using our *models as compressors*.

Let G_1 and G_2 be our input graphs with alignment \mathcal{A} and individual models M_1 and M_2 (encoded without node IDs). Let M_{12} be their best \mathcal{A} -respecting common model, and let Δ_1 and Δ_2 be transformations such that $\Delta_1(M_{12}) = M_1$ and $\Delta_2(M_{12}) = M_2$. The *Normalized Model Distance* (NMD) between G_1 and G_2 is

$$\text{NMD}(G_1, G_2) = \frac{L(M_{12}) + L(\Delta_1, \Delta_2) - \min\{L(M_1), L(M_2)\}}{\max\{L(M_1), L(M_2)\}}.$$

The NMD is 0 if $M_{12} = M_1 = M_2$ (with $\Delta_1 = \Delta_2 = \emptyset$), and it is 1 if $M_{12} = \emptyset$ (with $\Delta_1 = M_1$ and $\Delta_2 = M_2$). It allows us to compare our method with other similarity *measurement* methods even though our primary goal is similarity *description*, which we formalize next.

3.4 Similarity Description, Formally

We are now ready to formally state our problem.

THE GRAPH SIMILARITY DESCRIPTION PROBLEM. *Given graphs G_1, G_2 , and a (full, partial, or empty) alignment $\mathcal{A} : V_1 \rightarrow V_2$, find individual models M_1, M_2 , common model M_{12} , and transformations Δ_1, Δ_2 minimizing $L(M_{12}) + L(\Delta_1, \Delta_2) + L(G_1 \parallel_{\mathcal{A}} G_2 \mid M_{12}, \Delta_1, \Delta_2)$.*

The search space is huge: Even if we searched for *one* individual model only, limited the number of structures to k , set the minimum size of a structure to r , and required the union of all structures to form a partition of V , we would need to search over 4^k times the number of partitions of n into k parts of size at least r . These partitions are in bijection with the partitions of $n - k(r - 1)$ into k parts, and hence, there are $S(n - k(r - 1), k)$ of them, where S is the Stirling number of the second kind. Since we are looking for *three* models with intricate interconnections, the search space for our problem is even larger—not to mention the NP-hard subproblems we need to solve to identify optimal structures (e.g., MAXCLIQUE). Furthermore, our search space exhibits no structure such as (weak) (anti-)monotonicity of the total description length that would allow us to search it efficiently. Hence, we resort to heuristics.

4 ALGORITHM

We now introduce our second contribution, an algorithmic framework, called MOMO (*Model of models*), to approximate the graph similarity description problem. To discover good models in practice, we break this problem into two parts:

- (1) Approximate the individual models M_1 and M_2 minimizing $L(M_1) + L(G_1 \mid M_1)$ and $L(M_2) + L(G_2 \mid M_2)$. Since these models can be thought of as graph summaries, we refer to this task as *graph summarization*.
- (2) Given individual models M_1 and M_2 , approximate the common model M_{12} and the associated transformations Δ_1 and Δ_2 minimizing $L(M_{12}) + L(\Delta_1, \Delta_2) + L(G_1 \parallel_{\mathcal{A}} G_2 \mid M_{12}, \Delta_1, \Delta_2)$. Since we require there to be a unique structure in both M_1 and M_2 for each structure in M_{12} , this means we search for an optimal alignment between the structures in M_1 and M_2 . Hence, we refer to this task as *model alignment*.

Given $M_1, M_2, M_{12}, \Delta_1$, and Δ_2 , the NMD can be readily computed.

Our architecture is flexible in that (1) any algorithm generating graph summaries using the structure vocabulary Ω can be used in the first step, (2) any algorithm finding a common model and transformations based on individual graph summaries using the structure vocabulary Ω and the transformation vocabulary Σ can be used in the second step, and (3) all alphabets can be replaced with other alphabets (if they are mutually compatible and the encoding is suitably amended), just as the NMD can be substituted with an alternative measure, e.g., to adapt our method to a specific domain.

4.1 Step One: Graph Summarization (BEPP0)

We begin by summarizing each of our input graphs individually. That is, our input is a single graph G with node set V and edge set E , and our output is a model M approximately minimizing $L(M) + L(G \mid M)$. Our procedure, called BEPP0, is given as Algorithm 1.

To start, we decompose our graph into a set C of connected components of diameter at most three (l. 1). We do this by iteratively selecting the node v with the highest degree in the currently largest connected component to form a component $C \in \mathcal{C}$ with its neighbors, then deleting all edges incident with v , until no more components can be formed. This procedure is similar to the SLASH-BURN algorithm [18], but we recurse on the *globally*, rather than the *locally* largest connected component to ensure that all our components have small diameter. The generated components are used as seeds to produce candidates for each structure type from our structure vocabulary Ω , where we merge candidates of the same type if they overlap on a large fraction of their nodes (l. 3–7). We sort the remaining candidates, which can overlap on nodes *and edges*, from largest to smallest (l. 8). Finally, for each structure s , in order, we add s to M if this reduces our description length (l. 9–11), i.e., if $L(s) + L(G | M \cup \{s\}) < L(G | M)$.

To generate a candidate of a certain structure type from a given component C with node set V_C (l. 5), we proceed as follows.

For a *clique* with node set V_s , we first find the maximum clique in C and include its nodes in V_s , then we iteratively add the node from $V \setminus V_s$ with the highest degree in G that is connected to at least 50% of the nodes in V_s until no more nodes fulfill this criterion.

For a *star* with spoke set V'_s , we declare a node with the highest degree in C to be the hub v , set $V'_s = V_C \setminus \{v\}$, and then iteratively (1) identify the nodes in V'_s that have more than $0.05 \cdot |V'_s|$ neighbors in V'_s , and (2) remove the $\min\{(0.1 + 0.01i), 1\}$ fraction of these nodes from V'_s that has the most neighbors in V'_s in iteration i .

For a *biclique* with node sets L and R , to start, we set the right node set to be the (at most) 5 nodes in a *maximal* independent set (MIS) of V_C that have the highest degree in G . We then identify the set $L' \subseteq V \setminus R$ of nodes that are connected to at least 50% of the nodes in R , and set L to be the (at most) 5 nodes in an MIS of L' that have the highest degree in G . If $|L| < 3$ or $|R| < 5$, we discard the candidate early. For the surviving candidates, we then iteratively (1) identify the set X of nodes from $V \setminus (L \cup R)$ that are connected to at most 5% of the nodes in L and at least 50% of the nodes in R , adding to L the node from X (if any) with the most neighbors in R , and (2) perform (1), switching the roles of L and R , until no more nodes satisfy our criteria for addition to L or R .

For a *starclique* with node sets L and R , to start, we set L to be the set of nodes contained in the maximum clique of C . We then identify the set $R' \subseteq V \setminus L$ of nodes that are connected to at least 50% of the nodes in L , and set $R = \text{MIS}(R')$. Subsequently, we iteratively (1) identify the set X of nodes from $V \setminus (L \cup R)$ that are connected to at least 50% of the nodes in L and to at least 50% of the nodes in R , adding to L the node from X (if any) with the most neighbors in R , and (2) identify the set Y of nodes from $V \setminus (L \cup R)$ that are connected to at most 5% of the nodes in R and to at least 50% of the nodes in L , adding to R the node from Y (if any) with the most neighbors in L , until no more nodes can be added.

Running BEPPO on the graphs G_1 and G_2 , we obtain interpretable individual models M_1 and M_2 . Our next task is to align these models.

4.2 Step Two: Model Alignment (GIGI)

For the model alignment step, our inputs are the graphs G_1, G_2 , the node alignment \mathcal{A} , and the models M_1, M_2 . Our outputs are

Algorithm 1: Graph summarization with BEPPO

Input: Graph G ; structure vocabulary Ω
Output: Model M with structure list S

- 1 $C \leftarrow$ Connected components of G from decomposition
- 2 $S', S \leftarrow [], []$
- 3 **forall** structure types $\omega \in \Omega$ **do**
- 4 **forall** components $C \in \mathcal{C}$ **do**
- 5 Generate candidate of type ω from C
- 6 Merge generated candidates if they have large overlap
- 7 Append remaining candidates to S'
- 8 Sort structures $s \in S'$ by (n_s, m_s) (descending)
- 9 **forall** structures $s \in S'$ **do**
- 10 **if** $L(s) + L(G | M \cup \{s\}) < L(G | M)$ **then**
- 11 Append s to S
- 12 **return** M

Algorithm 2: Model alignment with GIGI

Input: Individual models M_1, M_2 with structures S_1, S_2 ;
node alignment \mathcal{A} ; transformation vocabulary Σ
Output: Common model M_{12} and transformations Δ_1, Δ_2
such that $\Delta_1(M_{12}) = M_1, \Delta_2(M_{12}) = M_2$

- 1 Compute constrained matching $\mathcal{M} \subseteq S_1 \times S_2$ // Alg. 3
- 2 $M_{12}, \Delta_1, \Delta_2 \leftarrow [], [], []$
- 3 **forall** structures $(s_1, s_2) \in \mathcal{M}$ **do**
- 4 Compute the common structure s for (s_1, s_2)
- 5 Compute δ_i such that $\delta_i(s) = s_i$ for $i \in \{1, 2\}$
- 6 Append s to M_{12} and δ_i to Δ_i for $i \in \{1, 2\}$
- 7 **for** $i \in \{1, 2\}$ **do**
- 8 **forall** structures $s \in S_i \setminus \{s \in S_i \mid \exists p \in \mathcal{M} : s \in p\}$ **do**
- 9 Append s to Δ_i
- 10 **return** $M_{12}, \Delta_1, \Delta_2$

a common model M_{12} and the transformations Δ_1, Δ_2 , which together minimize $L(M_{12}) + L(\Delta_1, \Delta_2) + L(G_1 \parallel_{\mathcal{A}} G_2 \mid M_{12}, \Delta_1, \Delta_2)$ approximately. Our procedure, called GIGI, is given as Algorithm 2.

In the critical first step, detailed below, GIGI computes a (bipartite) matching $\mathcal{M} \subseteq S_1 \times S_2$, pairing structures in S_1 with structures in S_2 (l. 1). The matching is *constrained* because we require that paired structures have the same type $\omega \in \Omega$. For each structure pair $(s_1, s_2) \in \mathcal{M}$, we then compute its common structure s as well as transformations δ_1 and δ_2 such that $\delta_1(s) = s_1$ and $\delta_2(s) = s_2$, which we add to M_{12}, Δ_1 , and Δ_2 , respectively (l. 3–6). Finally, we add the unpaired structures from both S_1 and S_2 to Δ_1 and Δ_2 , ensuring that $\Delta_1(M_{12}) = M_1$ and $\Delta_2(M_{12}) = M_2$ (l. 7–9).

Typically, the matching \mathcal{M} is not uniquely defined. We are interested in the matching that helps us minimize the description length. Sweeping the search space naively is not an option: For a structure vocabulary Ω , there exist $\prod_{\omega \in \Omega} (\omega_{\max} - \omega_{\min})! \cdot \binom{\omega_{\max}}{\omega_{\min}}$ different *maximal* matchings alone, where, for $f \in \{\min, \max\}$, $\omega_f = f\{\{s \in S_1 \mid \text{type}(s) = \omega\}, \{s \in S_2 \mid \text{type}(s) = \omega\}\}$. Hence,

we propose a matching heuristic, MAXIMALGREEDY, whose detailed pseudocode is given as Algorithm 3 in the Appendix.

If no node alignment is present, for $i \in \{1, 2\}$, MAXIMALGREEDY constructs *node overlap graphs* H_i . The nodes of these graphs are the structures in S_i , and the weights of their edges F_i are the Jaccard similarities between the node sets of the structures (l. 3). MAXIMALGREEDY then builds a variant of the *product graph* of H_1 and H_2 , whose nodes are the subset of $S_1 \times S_2$ that agrees on type, and whose edge weights are the product of the edge weights in H_1 and H_2 (l. 4–6). MAXIMALGREEDY then iteratively selects the heaviest edges in the product graph and removes all nodes that are incompatible with these edges (l. 7–12). Finally, it pairs the remaining structures of the same type in descending order of their size (l. 13–19).

If a (partial) node alignment \mathcal{A} is present, MAXIMALGREEDY iteratively matches those structures s_1 and s_2 of the same type whose node sets have the largest average Jaccard similarity under \mathcal{A} (l. 20–27). For cliques, this equals the standard Jaccard similarity. For structures of other types, it is defined as

$$\text{Jaccard}_{\mathcal{A}}(s_1, s_2) = \frac{1}{2} \cdot \sum_{i \in \{1, 2\}} \frac{|\mathcal{A}(V_i(s_1)) \cap V_i(s_2)|}{|\mathcal{A}(V_i(s_1)) \cup V_i(s_2)|},$$

where V_1 and V_2 are the hub and spoke sets (for stars) or the left and right node sets (for bicliques and starcliques), respectively.

MAXIMALGREEDY is designed to ensure interpretability: In the presence of a node alignment, it honors the node overlap of structures *between* graphs, and in the absence of such an alignment, it honors the node overlap of structures *within* graphs, all while respecting the constraints imposed by the structure types.

4.3 Computational Complexity

Having specified BEPPO and GIGI as the main components of MOMO, we now analyze MOMO’s complexity. Here, we assume that the total number of structures is $O(1)$, which is required for interpretability.

For BEPPO, due to the set intersection operations involved, constructing structure candidates is $\tilde{O}(nm)$, where \tilde{O} hides polylogarithmic factors. To decide whether to add a candidate to our model, we need to find the maximum entropy distribution for the adjacency matrix of the graph given that model, which is $O(1)$ since the number of Lagrange multipliers is $O(1)$. We also need to keep track of the mapping of Lagrange multipliers to potential edges, which is $O(n^2)$ with $O(1)$ candidates. Hence, BEPPO runs in $\tilde{O}(nm)$.

GIGI’s complexity is driven by $O(1)$ Jaccard similarity computations, which together take $O(n^2)$ in the worst case ($O(n)$ on average), where $n = \max\{n_1, n_2\}$. Given individual models M_1, M_2 , and their model alignment $(M_{12}, \Delta_1, \Delta_2)$, computing the NMD takes $O(1)$ basic arithmetic operations, i.e., its total complexity is $O(1)$.

Overall, MOMO’s complexity is dominated by BEPPO, and hence $\tilde{O}(nm)$ in the worst case. However, as we show in Section 6, in practice, MOMO’s performance is near-linear in the number of edges.

5 RELATED WORK

To the best of our knowledge, we are the first to treat graph similarity assessment primarily as a *description* problem, rather than as a *measurement* problem. Related work broadly falls into two categories: graph similarity measurement and graph summarization.

Graph Similarity Measurement. Early work on graph similarity measurement uses *global* measures that capture graph *structure*, e.g., graph edit distance and maximum common subgraphs [11, 22, 29]. Later research also explores measures that capture graph *connectivity* [14], leverage graph *decompositions* [20], or aggregate *local* similarities via node feature distributions [1, 2]. Building on prior work concerning *graph kernels* [3, 25], recent contributions investigate similarity learning via *deep* graph kernels [19, 21, 27, 28].

In contrast to the existing literature, first, our *primary goal* is graph similarity *description*, not *measurement*. Second, our *perspective* emphasizes *interpretability*, which leads us to build on intuitive meso-level structures, rather than (overwhelmingly numerous) micro-level node features, motifs, or (opaque) macro-level graph features. Third, our *approach* is novel in that it formalizes graph similarity as a model selection task using the MDL principle.

When evaluating MOMO, we compare the NMD to another normalized similarity measure that is also based on information-theoretic principles: the *Network Portrait Divergence* (NPD) [1]. The NPD is the Jensen-Shannon divergence of the probability distributions of the input graphs that describe how many nodes have x neighbors at distance y . We show that the NMD and the NPD often capture similar trends, but only the NMD is intuitively interpretable.

MDL-Based Graph Summarization. Although novel in graph similarity assessment, the MDL principle has been used extensively in graph summarization. Starting with the SUBDUE system [4], a rich line of work has sought to move summarization beyond clustering using more expressive vocabularies to identify meaningful structures in *static* graphs [8, 9, 13, 18]. MDL has also been used to find partitions in graph *streams* [26] or structures ranging across multiple *aligned* snapshots of *dynamic* graphs [12, 24].

Going beyond the existing literature, first, we allow our structures to overlap not only on nodes but also on *edges*, and we can handle multiple graphs even if they are *unaligned*. Second, we improve the *methodology* of previous static summarization methods, leveraging more noise-tolerant structure definitions and an optimal encoding of the data under the model. Third, in our structure search, we emphasize result *quality*, reflecting the need for accurate graph summaries as inputs to our comparison algorithm.

When evaluating MOMO, we compare BEPPO to VoG [13], a static graph summarizer built on a similar graph decomposition method and vocabulary of interpretable structures (including cliques, bicliques, stars, and chains) that neither uses maximum entropy modeling or component post-processing nor allows edge overlap. We show that BEPPO discovers more informative summaries than VoG.

6 EXPERIMENTS

We now present our third contribution, an extensive evaluation of the framework presented in Section 4. To this end, we implement BEPPO in Julia and all other parts of MOMO in Python. We run our experiments on Intel E5-2643 CPUs with 256 GB RAM. All data, code, and results are publicly available.² We answer three questions:

- Q1 Does BEPPO create useful graph summaries?
- Q2 Does GIGI discover interpretable common models?
- Q3 Does MOMO yield informative similarity scores?

²<http://eda.mmci.uni-saarland.de/prj/momo>; <https://doi.org/10.5281/zenodo.4780912>

To ensure interpretability, we limit our summaries to at most 100 structures, although allowing more would give better compression.

In our experiments, we use real-world graphs from seven collections (cf. Appendix Table 3): Graphs in the *asb* and *asp* collections represent peering relations between Autonomous Systems, each in 9 different weeks from 2001 [15]; graphs in the *bio* collection represent physical interactions between human proteins in 144 different tissues, where the protein identities induce partial node alignments between all pairs of graphs in the collection [30]; graphs in the *clg* and *csi* collections represent arXiv collaboration networks of cs.LG and cs.SI in each year from 2011 to 2020 [5]; and graphs in the *lus* and *lde* collections represent references between sections of the United States Code and the Code of Federal Regulations or their German equivalents in each year from 1998 to 2019 [6]. We also include two collections of synthetic random graphs, *rba* and *rer*, based on the Barabási-Albert (BA) model and the Erdős-Rényi (ER) model. Our graphs vary in size and density, containing up to 160K nodes and up to 525K edges (cf. Appendix Figure 10).

Q1: Does BEPPO create useful graph summaries? In our context, graph summaries are useful if they capture the essence of a graph in an easily comprehensible manner. To assess whether BEPPO creates such summaries, we start by comparing with VoG, which has been shown to produce useful graph summaries, on graphs from the VoG paper [13]. As shown in Table 1, in all experiments, BEPPO saves more bits relative to the original encoding length than VoG-*k* for the same *k*, i.e., it achieves a better compression *L%*. Moreover, BEPPO’s compression is comparable to that of VoG-Greedy, although it uses much fewer structures. That is, even though our encoding of the data under the model is optimal, we manage to save more bits per structure than VoG. We also observe that while BEPPO uses its entire vocabulary to summarize its input graphs, VoG finds almost only stars. As we show in Figure 3, despite doing more work than VoG, BEPPO is near-linear in practice.

In the left panel of Figure 4, we tally how many structures of each type we find and what compression we achieve, on average, in each graph from our collections. Since the edges of ER graphs are chosen uniformly at random, and BA graphs are grown using preferential attachment, it comes as no surprise that we find at most one star (with minimal gain) in ER graphs and only stars in BA graphs, achieving no or little compression. The highest fraction of cliques occurs in the collaboration graphs (*clg*, *csi*), where papers with many authors induce cliques. The hubs of the stars in these graphs correspond to well-known researchers with many independent collaborations, e.g., *Yoshua Bengio*, *Yang Liu*, and *Sergey Levine* in *clg* 2020. Some researchers occur in several structures, e.g., in *csi* 2020, 6 of the spokes in the star around *Christos Faloutsos*, shown in the right panel of Figure 4, reappear in the star around *Danai Koutra*, and some of them are also connected. This demonstrates the importance of allowing structures to overlap on nodes and on edges, a feature absent from other state-of-the-art summarizers like VoG. For the law graphs (*lde*, *lus*), analysis by the first author (who happens to hold a PhD in law) and discussion with legal scholars revealed that we can classify stars based on the ratio of the in- and out-degree of their hubs to uncover their legal function. Thus, BEPPO produces summaries that are useful to domain experts even for *directed* graphs, which sets it further apart from other methods.

Table 1: BEPPO compresses graphs more efficiently than VoG. $|S|$ is the number of structures, and $L%$ is the compression (in percent of the uncompressed encoded length).

Graph	<i>n</i>	<i>m</i>	BEPPO		VoG- <i>k</i>		VoG-G	
			$ S $	$L%$	$ S $	$L%$	$ S $	$L%$
Epinions	75879	405740	100	20	100	5	2746	19
Enron	79870	288364	100	18	100	7	2331	25
AS-Oregon	13579	37448	100	28	100	21	399	29
Chocolate	2877	5467	55	9	100	7	101	12
Controversy	1093	2942	20	15	100	4	35	13

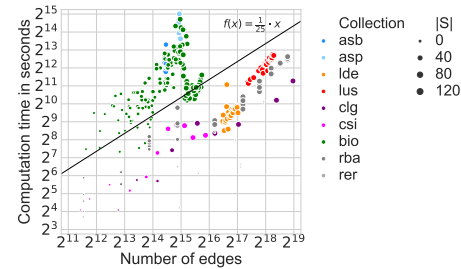
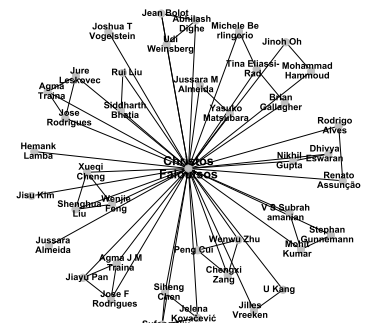


Figure 3: BEPPO is near-linear and output-sensitive. Its computation time is shown as a function of *m*, with markers scaled by the number of discovered structures $|S|$.

Coll.	\widehat{cl}	\widehat{st}	\widehat{bc}	\widehat{sc}	$\widehat{L\%}$
asb	1	96	0	1	29
asp	3	91	0	6	29
bio	6	52	1	2	9
clg	24	36	0	2	8
csi	13	48	0	1	16
lde	0	98	1	1	1
lus	0	95	4	1	4
rba	0	68	0	0	3
rer	0	1	0	0	0



Results of BEPPO

Example star from csi 2020

Figure 4: BEPPO identifies meaningful structures. We show its average compression and number of structures per type (left), and an example star discovered in *csi* 2020 (right).

Since we allow structures to overlap, BEPPO’s summaries can be visualized intuitively as *node overlap trees*. Node overlap trees are the maximum spanning trees of node overlap graphs, i.e., each vertex in them represents a structure, the edge weights are the Jaccard similarities between the node sets of the structures, and we remove all edges that are lightest in a cycle. To ensure connectivity, we introduce a root vertex that connects to the vertex with the largest degree inside each component. We depict the node overlap trees for selected digestive tract tissues from the *bio* collection in Figure 5. Here, larger shapes indicate larger structures, and thicker edges indicate higher Jaccard similarities. From the vertices and the connectivity structure of the trees, it is immediately apparent that the top-row tissues are very similar, and indeed, the functions performed by the organs they represent are closely related.

Q2: Does GIGI discover interpretable common models? As GIGI builds on BEPPO, the common models it discovers are composed of easily comprehensible structures. By construction, this ensures a certain degree of interpretability. To understand the composition of a common model M_{12} and its relationship to individual models M_1 and M_2 , we can further visualize these models using treemaps. We show an example from the *bio* collection in Figure 6, contrasting the individual models for esophagus and colon with their common model. We see that esophagus and colon have many common structures, most of them stars, but the esophagus has more complex or dense structures (cliques, bicliques, and starcliques), while the colon has more simple sparse structures (stars). Using the node alignments between the *bio* graphs to annotate the shared structures with their average Jaccard similarities, we observe that all stars that are shared between esophagus and colon have a shared hub (indicated by a similarity above 0.5). Similar observations can be made for other tissues, e.g., the largest cliques in the top-row tissues from Figure 5 all have a Jaccard similarity of at least 0.58. This indicates that *housekeeping proteins* might be expressed as *housekeeping structures* that recur across tissues, but a detailed investigation of this hypothesis lies outside the scope of this paper.

Beyond bilateral graph similarity assessment, GIGI’s output enables comparisons between multiple graphs. As an example, in Figure 7, we display the composition of the common models for comparisons of the esophagus with the tissues from Figure 5 as a triptych of stacked bar charts. The graphic illustrates that the relationship between esophagus and colon, shown in Figure 6, is comparable to that of the esophagus and *any* top-row organ from Figure 5, and that all bottom-row organs share a biclique structure.

To further explore the relationships between shared structures, we can leverage *common* node overlap graphs, i.e., node overlap graphs induced by our structure matching \mathcal{M} , with nodes $(s_1, s_2) \in \mathcal{M}$, edges $((s_1, s_2), (t_1, t_2))$, and edge weights $\prod_{i \in \{1,2\}} \text{Jaccard}(s_i, t_i)$. These graphs convey an interpretable notion of equivalence between the matched structures. To visualize common node overlap graphs, we again use node overlap trees, and Figure 11 in the Appendix shows an example from the *lde* collection. While not all patterns from the individual trees recur in the common tree, the trees induced by the common tree in the individual node overlap graphs typically weigh a large fraction of the individual node overlap trees, i.e., the alignments discovered by GIGI respect much of the node overlap shared between the structures in our input graphs.

Q3: Does Momo yield informative similarity scores? Although our focus is similarity *description*, we can also use our similarity score, the NMD, for similarity *measurement*. As depicted in Figure 12 in the Appendix, experiments on synthetic models show that the NMD is almost scale-invariant when the graphs contain rescaled versions of the same structures and their size differs within one order of magnitude, with larger size differences leading to larger NMD values. The NMD also behaves intuitively for models of varied compositions, showing a strong correlation with the number of structures that can be matched across graphs.

When we compare NMDs to *Network Portrait Divergence* values (NPDs), on the yearly snapshots of the IBM GitHub collaboration network from 2013 to 2017 used in [1], the general trends are quite similar, but some years are *more* similar and others are *less* similar

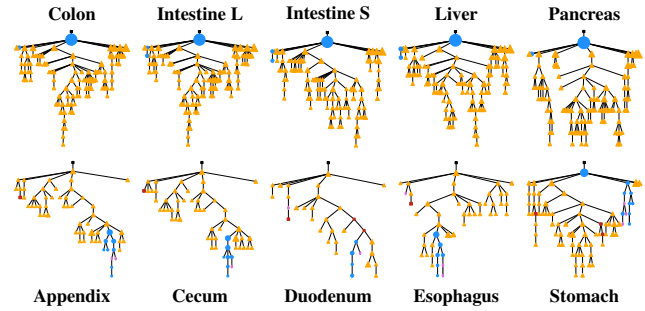


Figure 5: BEPPO creates similar summaries with similar node overlap structure for similar graphs. The node overlap trees for selected digestive tract organs in the *bio* collection mirror the functional (dis)similarity between these organs.

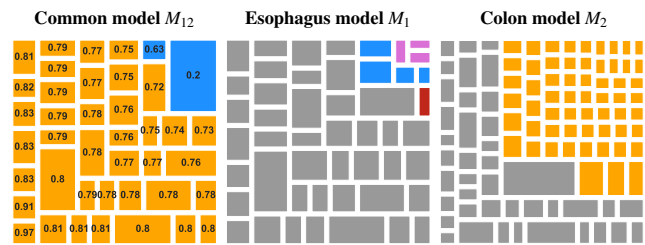


Figure 6: GIGI discovers interpretable common models. The common model (left) for esophagus (middle) and colon (right) contains mostly structures with high average Jaccard similarity (annotations). Each rectangle corresponds to a structure, sized proportionally to its number of nodes, and shared structures are greyed out in the individual models.

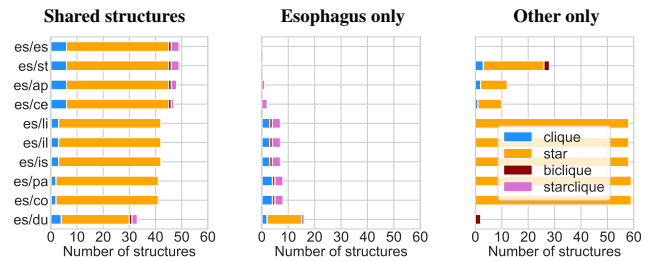


Figure 7: GIGI allows multi-graph comparisons. Here, we juxtapose shared (left) and specific (middle, right) structures for the esophagus and the tissues from Figure 5.

under NMD than under NPD (cf. Appendix Figure 13). However, only our results are also interpretable: In 2014, for example, the network only has one star structure, explaining its high dissimilarity to 2015, which features one starclique and two cliques. The differences between NMD values and NPD values are likely due to the dependence of NPD on graph size, but since the underlying statistics are not intuitively comprehensible, we cannot be sure.

In Figure 8, we depict the distribution of NMDs for all pairwise comparisons of *different* graphs in our real-world collections. We see that NMDs span the whole range, and their distribution differs depending on the type of comparison (*cross-sectional* vs.

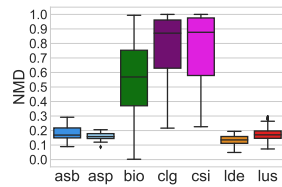


Figure 8: NMDs are lower for cross-temporal comparisons of systems experiencing gradual change (*asb, asp, lde, lus*) than for cross-temporal comparisons of systems undergoing radical change (*clg, csi*) or cross-sectional comparisons (*bio*).

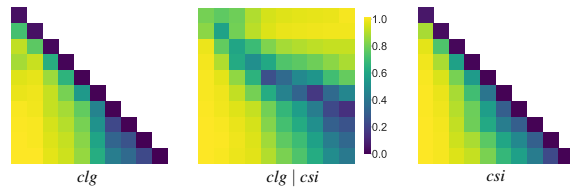


Figure 9: NMDs yield nuanced insights. The NMDs for the *clg* and *csi* graphs from 2011 (top/left) to 2020 (bottom/right) show the arrow of time within each collection (left, right) and the lag between *clg* and *csi* from 2015 onwards (middle).

cross-temporal) and the type of change (*gradual* vs. *radical*) experienced by the system we study. To illustrate radical change, we show the NMDs of the collaboration graphs (*clg, csi*) from 2011 to 2020 in Figure 9. Both collections display the arrow of time, but self-similarity drops faster in *clg* than in *csi* from about 2015 onwards, and when comparing across collections, *csi* 2015 is most similar to *clg* 2015 but *csi* 2020 is most similar to *clg* 2017. Thus, while both communities have picked up tremendous pace in the past ten years, development in *clg* has been measurably more rapid than in *csi*.

7 CONCLUSION

We study graph similarity assessment as a *description* problem, guided by the question “*how* are these graphs similar?”. Formalizing the problem using the MDL principle, we capture the similarity of the input graphs in their *common model* and the differences between them in *transformations to individual models*. Since our search space is huge and unstructured, we propose a framework, MOMO, which breaks the problem into two parts: BEPPO creates graph summaries that are useful to domain experts, and GIGI discovers interpretable common models, from which we can also derive informative similarity scores. Through experiments on undirected and directed graphs of radically varying sizes from diverse domains, we confirm that MOMO works well and is near-linear in practice.

However, MOMO also leaves room for improvement. For example, we would like to handle richer graph types, including weighted and attributed graphs, using encodings that fully leverage the available information. Ideally, BEPPO and GIGI would discover their structure and transformation vocabularies on the fly, integrating domain-specific background knowledge in the process. An improved structure encoding might account for the overlap between structures, which is currently considered explicitly only by GIGI. Our NMD score focuses on the models of the input graphs, and a more comprehensive measure could integrate the data under these models.

Finally, MDL forces us to take a binary decision when considering structure candidates, which can result in large differences between models based on small differences between description lengths. To eliminate these artifacts and still retain interpretability, we could consider the full set of high-quality structure candidates and compress it using *structures of structures*. This could lead to an *interpretable graph kernel*, which—like overcoming MOMO’s other limitations—constitutes an engaging topic for future work.

REFERENCES

- [1] J. P. Bagrow and E. M. Bollt. 2019. An information-theoretic, all-scales approach to comparing networks. *Applied Network Science* 4, 1 (2019), 45:1–45:15.
- [2] M. Berlingerio, D. Koutra, T. Eliassi-Rad, and C. Faloutsos. 2013. Network similarity via multiple social theories. In *ASONAM*. ACM, 1439–1440.
- [3] K. M. Borgwardt and H.-P. Kriegel. 2005. Shortest-path kernels on graphs. In *ICDM*. IEEE, 8 pp.
- [4] D. J. Cook and L. B. Holder. 1994. Substructure Discovery Using Minimum Description Length and Background Knowledge. *JAIR* 1 (1994), 231–255.
- [5] Cornell University. 2020. arXiv Dataset, Version 18 (2020/11/22). (2020). <https://www.kaggle.com/Cornell-University/arxiv>
- [6] C. Coupette, J. Beckedorf, D. Hartung, M. Bommarito, and D. M. Katz. 2021. Measuring Law Over Time. *Frontiers in Physics* (2021). DOI: <http://dx.doi.org/10.3389/fphy.2021.658463>
- [7] T. De Bie. 2011. Maximum entropy models and subjective interestingness: an application to tiles in binary databases. *Data Min. Knowl. Disc.* 23, 3 (2011), 407–446.
- [8] J. Feng, X. He, N. Hubig, C. Böhm, and C. Plant. 2013. Compression-based graph mining exploiting structure primitives. In *ICDM*. IEEE, 181–190.
- [9] S. Goebel, A. Tonch, C. Böhm, and C. Plant. 2016. MeGS: Partitioning meaningful subgraph structures using minimum description length. In *ICDM*. IEEE, 889–894.
- [10] P. Grünwald. 2007. *The Minimum Description Length Principle*. MIT Press.
- [11] F. Kaden. 1990. Graph distances and similarity. In *Topics in Combinatorics and Graph Theory*. Springer, 397–404.
- [12] S. Kapoor, D. K. Saxena, and M. van Leeuwen. 2020. Online summarization of dynamic graphs using subjective interestingness for sequential data. *Data Min. Knowl. Disc.* 35, 1 (2020), 1–39.
- [13] D. Koutra, U. Kang, J. Vreeken, and C. Faloutsos. 2015. Summarizing and understanding large graphs. *Stat. Anal. Data Min.* 8, 3 (2015), 183–202.
- [14] D. Koutra, N. Shah, J. T. Vogelstein, B. Gallagher, and C. Faloutsos. 2016. DeltaCon: principled massive-graph similarity function with attribution. *ACM TKDD* 10, 3 (2016), 1–43.
- [15] J. Leskovec, J. Kleinberg, and C. Faloutsos. 2007. Graph evolution: Densification and shrinking diameters. *ACM TKDD* 1, 1 (2007), 2:1–2:41.
- [16] M. Li, X. Chen, X. Li, B. Ma, and P. Vitányi. 2004. The similarity metric. *IEEE TIT* 50, 12 (2004), 3250–3264.
- [17] M. Li and P. Vitányi. 1993. *An Introduction to Kolmogorov Complexity and its Applications*. Springer.
- [18] Y. Lim, U. Kang, and C. Faloutsos. 2014. SlashBurn: Graph compression and mining beyond caveman communities. *IEEE TKDE* 26, 12 (2014), 3077–3089.
- [19] G. Ma, N. K. Ahmed, T. L. Willke, and P. S. Yu. 2019. Deep Graph Similarity Learning: A Survey. (2019). [arXiv:cs.LG/1912.11615](https://arxiv.org/abs/1912.11615)
- [20] G. Nikolentzos, P. Meladianos, S. Limnios, and M. Vazirgiannis. 2018. A Degeneracy Framework for Graph Similarity. In *IJCAI*. 2595–2601.
- [21] S. Ok. 2020. A graph similarity for deep learning. In *NeurIPS*, Vol. 34.
- [22] J. W. Raymond, E. J. Gardiner, and P. Willett. 2002. Rascal: Calculation of graph similarity using maximum common edge subgraphs. *Comput. J.* 45, 6 (2002), 631–644.
- [23] J. Rissanen. 1983. A Universal Prior for Integers and Estimation by Minimum Description Length. *Annals Stat.* 11, 2 (1983), 416–431.
- [24] N. Shah, D. Koutra, T. Zou, B. Gallagher, and C. Faloutsos. 2015. Timecrunch: Interpretable dynamic graph summarization. In *KDD*. ACM, 1055–1064.
- [25] N. Shervashidze, S. Vishwanathan, T. Petri, K. Mehlhorn, and K. Borgwardt. 2009. Efficient graphlet kernels for large graph comparison. In *Artificial Intelligence and Statistics*. 488–495.
- [26] J. Sun, C. Faloutsos, S. Papadimitriou, and P. S. Yu. 2007. GraphScope: parameter-free mining of large time-evolving graphs. In *KDD*. 687–696.
- [27] M. Togninalli, E. Ghisu, F. Llinares-López, B. Rieck, and K. Borgwardt. 2019. Wasserstein weisfeiler-lehman graph kernels. In *NeurIPS*. 6439–6449.
- [28] P. Yanardag and S. Vishwanathan. 2015. Deep graph kernels. In *KDD*. ACM, 1365–1374.
- [29] Z. Zeng, A. K. Tung, J. Wang, J. Feng, and L. Zhou. 2009. Comparing stars: On approximating graph edit distance. *PVLDB* 2, 1 (2009), 25–36.
- [30] M. Zitnik and J. Leskovec. 2017. Predicting multicellular function through multi-layer tissue networks. *Bioinformatics* 33, 14 (2017), i190–i198.

A APPENDIX

In this Appendix, we provide further details on our algorithms, our data (i.e., graph collections), and our experiments. The basic notation used throughout our paper is summarized in Table 2. We make all our data, code, and results publicly available.³

Algorithms. In the following, we provide implementation details for all components of MOMO: BEPPO, GIGI, and the NMD computation.

BEPPO. BEPPO has a size threshold, which allows us to stop decomposing connected components or discard generated candidates when they are too small. We set this threshold to 10 for all our experiments except when comparing NMDs with NPDs, where we set it to 3 because the input graphs are relatively small.

When deciding whether to merge candidates due to large overlap between their node sets in the final candidate generation step, we choose our merge thresholds such that we can reduce redundancy amongst candidates without harming structure quality. For cliques, we set the merge threshold to 90% of the nodes. For bicliques and starcliques, we require both the left sets and the right sets of two candidates to overlap on 90% of the nodes. We do not merge stars even for large overlaps because this would result in structures of a different type, which we generate separately.

We allow BEPPO to stop early if (1) it has added a given maximum number of structures to our model, or (2) we have tested a given maximum number of candidates *without* adding them to our model. As described at the beginning of Section 6, to guarantee that our summaries are interpretable, we set their maximum number of structures to 100. We set the maximum number of rejected candidates to 300, but in our experiments, this becomes relevant only for graphs from the *bio* collection. Because these graphs are relatively dense, BEPPO creates many overlapping candidates, but few of them suffice to cover most of the nodes and edges. With early stopping, we can thus shorten the running time of BEPPO without compromising the quality of our graph summaries.

GIGI. In Section 4.2, we give a verbal description of the MAXIMALGREEDY matching heuristic used by GIGI. Supplementing this description, we provide the detailed pseudocode of MAXIMALGREEDY as Algorithm 3. To speed up the computation when no node alignment is given and structures do not overlap, our implementation has a no-overlap flag which, when set, allows us to skip directly to the greedy matching (l. 13–19).

NMD Computation. If we compute the NMD naively, it is in rare cases possible to obtain a value above 1. This occurs when the models for the two graphs are so different that encoding them individually is cheaper than encoding them using a common model and transformations, i.e., when $L(M_{12}) + L(\Delta_1, \Delta_2) > L(M_1) + L(M_2)$. As any value above 1 signals that we do not gain any bits by compressing G_1 and G_2 together, we set the NMD to 1 in this situation.

For the *bio* collection, the NMD distribution we report in Figure 8 is based on structure matchings using node alignments induced by protein identities. For all other collections, the distributions reported are based on structure matchings without node alignments.

Table 2: Basic notation.

Symbol	Description
$G_i = (V_i, E_i)$	graph i with node set (edge set) V_i (E_i)
$n_i = V_i $	number of nodes in G_i
$m_i = E_i $	number of edges in G_i
A_i	adjacency matrix of G_i
\mathcal{A}_{ij}	alignment between V_i and V_j
$L(x)$	number of bits to describe x using our encoding
$L_{\mathbb{N}}(x)$	number of bits to describe x using the universal code for integers
\log	binary logarithm with $\log(0) = 0$
$\lfloor x \rfloor$	x rounded to the closest integer

Algorithm 3: Structure matching with MAXIMALGREEDY

```

Input: Structure lists  $S_1, S_2$ ; node alignment  $\mathcal{A}$ 
Output: Structure matching  $\mathcal{M} \subseteq S_1 \times S_2$ 
1  $\mathcal{M} \leftarrow \emptyset$ 
2 if  $\mathcal{A} = \emptyset$  then
3    $H_i \leftarrow (S_i, F_i, w_i)$  for  $i \in \{1, 2\}$ ,  $w_i((s, t)) = \text{Jaccard}(s, t)$ 
4    $V \leftarrow \{(s_1, s_2) \in S_1 \times S_2 \mid \text{type}(s_1) = \text{type}(s_2)\}$ 
5    $E \leftarrow \{((s_1, s_2), (t_1, t_2)) \mid (s_1, t_1) \in F_1, (s_2, t_2) \in F_2\}$ 
6    $G \leftarrow (V, E, w)$ ,  $w(((s_1, s_2), (t_1, t_2))) = \prod_{i \in \{1, 2\}} w_i((s_i, t_i))$ 
7   while  $E \neq \emptyset$  do
8      $(u, v) \leftarrow \arg \max_{(u, v) \in E} w((u, v))$ 
9     Add  $u$  and  $v$  to  $\mathcal{M}$ 
10     $X \leftarrow \{x \in V \setminus \mathcal{M} \mid (x \cap u \neq \emptyset) \vee (x \cap v \neq \emptyset)\}$ 
11     $E \leftarrow E \setminus \{(u, v)\}$ 
12     $G \leftarrow G[V \setminus X]$ 
13   $\bar{S}_i \leftarrow S_i \setminus \{s \in S_i \mid \exists p \in \mathcal{M} : s \in p\}$  for  $i \in \{1, 2\}$ 
14  forall structures  $s_1 \in \bar{S}_1$  do
15    forall structures  $s_2 \in \bar{S}_2$  do
16      if  $\text{type}(s_1) = \text{type}(s_2)$  then
17        Add  $(s_1, s_2)$  to  $\mathcal{M}$ 
18         $\bar{S}_i \leftarrow \bar{S}_i \setminus \{s_i\}$  for  $i \in \{1, 2\}$ 
19        break
20 else
21    $\bar{S}_i \leftarrow S_i$  for  $i \in \{1, 2\}$ 
22   while true do
23      $U \leftarrow \{(s_1, s_2) \in \bar{S}_1 \times \bar{S}_2 \mid \text{type}(s_1) = \text{type}(s_2)\}$ 
24     if  $U = \emptyset$  then break
25      $(s_1, s_2) \leftarrow \arg \max_{(s_1, s_2) \in U} \text{Jaccard}_{\mathcal{A}}(s_1, s_2)$ 
26     Add  $(s_1, s_2)$  to  $\mathcal{M}$ 
27      $\bar{S}_i \leftarrow \bar{S}_i \setminus \{s_i\}$  for  $i \in \{1, 2\}$ 
28 return  $\mathcal{M}$ 

```

³<http://eda.mmci.uni-saarland.de/prj/momo>; <https://doi.org/10.5281/zenodo.4780912>

Table 3: Our experiments are based on graph collections from highly diverse domains. N is the number of networks in the respective collection.

Coll.	Description	N	Distinction	Source
asb	AS Oregon RouteViews basic	9	2001/03/31–05/26,	[15]
asp	AS Oregon RouteViews plus	9	weekly	
bio	physical protein interactions	144	human tissues	[30]
clg	arXiv cs.LG collaborations	10	2011–2020,	[5]
csi	arXiv cs.SI collaborations	10	yearly (11/01)	
lde	German federal law	22	1998–2019,	[6]
lus	United States federal law	22	yearly	
rba	Barabási-Albert random graphs	50	10 sizes,	–
rer	Erdős-Rényi random graphs	50	5 seeds	–

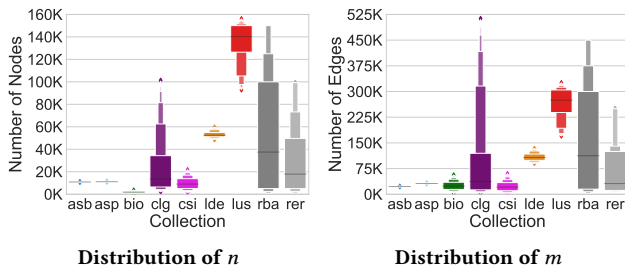


Figure 10: We consider graphs of radically varying sizes.

Data. Beyond the implementation details of our algorithms, to facilitate the interpretation of our results, we provide additional background on the graph collections we use in our experiments. Supplementing the description at the beginning of Section 6, we give an overview of our graph collections in Table 3, and show their distributions of n and m in Figure 10. For all collections except *asb* and *asp*, we perform some preprocessing to transform the data provided into the graphs we use, which is documented in our codebase. All random graphs are generated with graph generators available in the Python library `networkx`.

Experiments. We complete our additional remarks by delivering the details we deferred in Section 6. Full results for all our collections, including further visualizations, are provided along with our code.

When comparing BEPO with VoG in Table 1 of Q1, we state the n and m we found in the original input data, which sometimes differs slightly from those reported in [13].

As promised when answering Q2, we juxtapose common and individual node overlap trees for an example from the *lde* collection in Figure 11. Here, the trees induced by the common tree in the individual node overlap graphs weigh more than 4/5 of the individual node overlap trees.

Supplementing the discussion in Q3, in Figure 12, we provide a single-linkage hierarchical clustering of the NMDs of synthetic graphs with $n \in \cup_{i=1}^{10} \{i \cdot 10^4\}$ nodes that contain $\lfloor 100/|S| \rfloor$ structures of each type in S , for $S \in \mathcal{P}(\Omega) \setminus \emptyset$ (150 graphs in total). Finally, we visualize our comparison of NMDs with NPDs in Figure 13.

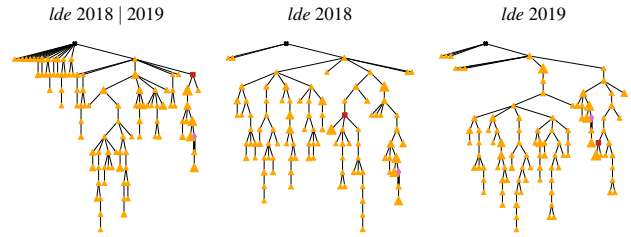


Figure 11: GIGI discovers common models retaining much of the node overlap shared by the structures in the individual graphs, as can be seen by comparing common (left) and individual (middle, right) node overlap trees.

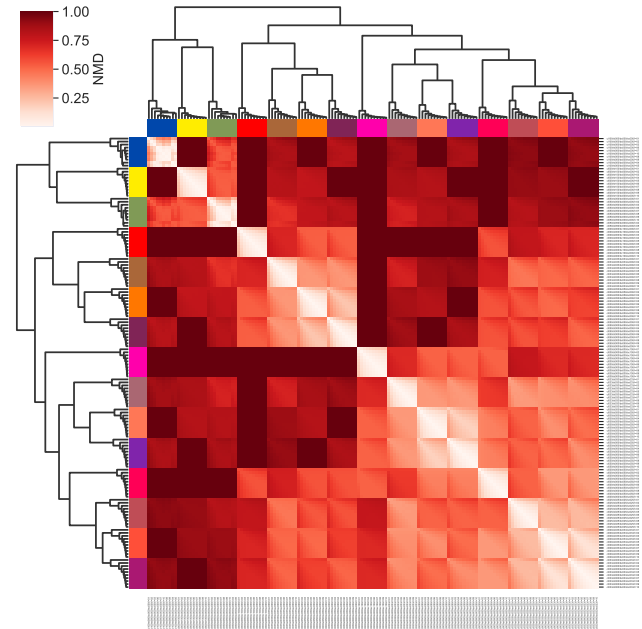


Figure 12: NMDs are (almost) scale-invariant (light strip along the diagonal) and correlate strongly with the number of structures that are matched across graphs (seven distinct shades of red). Row and column colors indicate model composition (mixed proportionally using blue, yellow, red, and magenta as the base colors for our structures); labels show structure counts per type and graph size (represented by i).

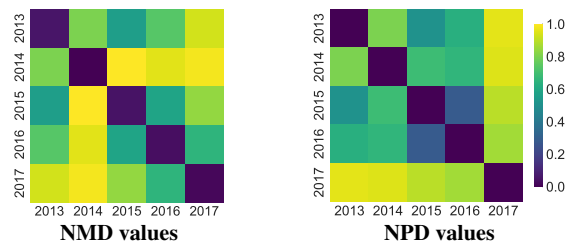


Figure 13: NMD and NPD detect similar trends, but where they differ, only NMD values are easy to interpret. Here, we compare NMD values (left) with NPD values (right) on the IBM GitHub collaboration network from [1].